UCRL--15419
EGG 1183-2432

EG&G

Energy Measurements Group

CLIMAX SPENT FUEL DOSIMETRY

PROGRESS REPORT

SEPTEMBER 1980 – SEPTEMBER 1981

OCTOBER 1981

WORK PERFORMED FOR THE U.S. DEPARTMENT OF ENERGY
UNDER CONTRACT NO. DE-AC08-76NV01183

SANTA BARBARA OPERATIONS
EG&G INC., 130 ROBIN HILL RD., GOLETA, CALIF. 93017

NOTICE

EG&G

Energy Measurements Group

EGG 1183-2432
S-720-R

UCRL--15419

DE86 011495

CLIMAX SPENT FUEL DOSIMETRY

PROGRESS REPORT

SEPTEMBER 1980 – SEPTEMBER 1981

by

W. Quam and T. DeVore

OCTOBER 1981

This report is unclassified: John Borella
Classification Officer

Work performed for the Lawrence Livermore National Laboratory
under SANL 909-034

SANTA BARBARA OPERATIONS
EG&G INC. 130 ROBIN HILL RD. GOLETA, CALIF 93017

FOREWORD

This report is one of a series covering dosimetry work at the Climax Spent Fuel Test Facility. The preceding progress report* described mechanical construction of the dosimeter holders. The present report covers the gamma and neutron data derived from the first dosimeter exchange (January, 1981). Future reports will cover subsequent dosimeter exchanges, nominally at 8-month intervals.

This work was done for Lawrence Livermore National Laboratory under SANL 909-034.

*Covered work up to February 1980. Informal report sent to customer only.

CONTENTS

ILLUSTRATIONS

TABLES

1. INTRODUCTION

This progress report covers work up to September, 1981. During this time the gamma calibrations were completed, the temperature-induced fading study was completed, the first set of exposed dosimeters was retrieved, and the second set of dosimeters was placed in the field. These were installed in stainless steel tubes located on the inside wall of five canister emplacement holes (0.61 m in diameter), numbers 1, 3, 4, 7, and 11. Hole 3 also had dosimeters in similiar stainless steel tubes placed at radii of 0.51 and 0.66 m from the canister centerline.

Data obtained from the first exposure (about 270 days in duration) are reported. Significant neutron exposures were measured; in some cases they were sufficiently high that neutron spectra could be calculated.

For a description of the hardware used in the field exposures, please refer to the previous informal progress report, dated 7 February 1980.

2. GAMMA DOSIMETRY SYSTEM

The gamma dosimetry system selected for this task uses radiation-induced color centers formed in optical grade ^{7}LiF. Literature references[1,2] suggested that this system is capable of response beyond 10^{8} rads and should exhibit little fading at temperatures >50°C. We verified these data and extended the fade tests to 150°C (see Section 2.2).

As noted in the 7 February 1980 progress report, the ^{7}LiF was prepared by Harshaw Chemical in the form of 2 × 2 × 5 mm right parallelpiped prisms, the size dictated by physical limitations of the space available for dosimetry. These clear small chips darken with exposure, and are very dark brown at 10^{8} rads. The absorption spectra shown in Figure 1, measured with a Beckman 5270 spectrophotometer, show peaks at wavelengths of 247, 374, and 443 mm, corresponding to

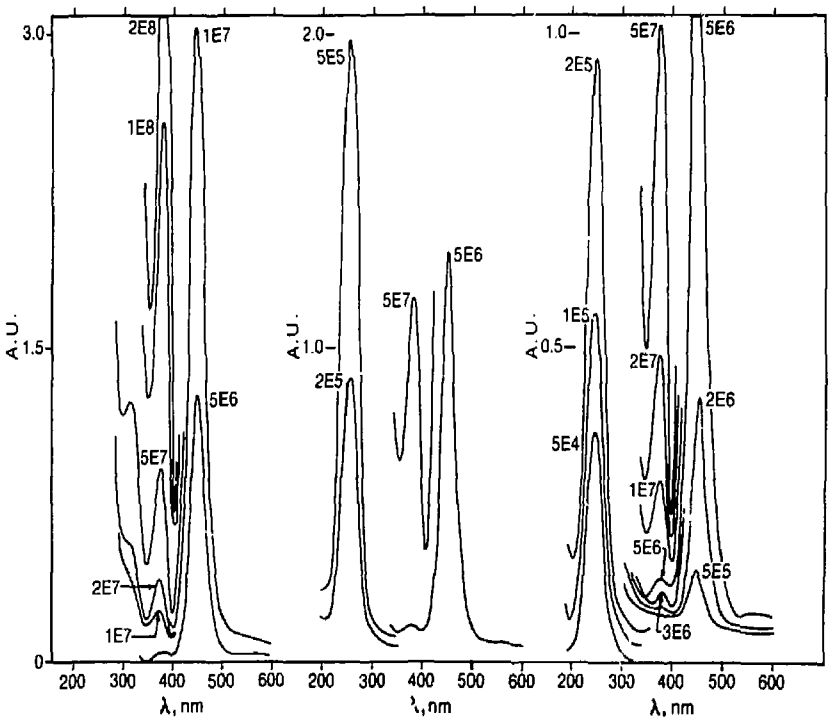

Figure 1. Spectrophotometer traces of ^{7}LiF chips at several dose levels and 0-1, 0-2, and 0-3 Absorbance Units (A.U.) scales

color centers named F, R_2, and M, respectively. Other color centers have been reported in the literature, but of these only N_2 was important under our experimental conditions. Table 1, adapted from McLaughlin, et al,[1] shows some of the characteristics of these color centers. The number of trapped electrons in each

Table 1. LiF color center data

Color Center Name	F^- Ion Vacancies	Trapped Electrons	Wavelength (nm)	Ranked Neutron Sensitivity
F	1	1	247	1 (least)
R_2	3	3	371	3
M	2	2	445	2
N_1,N_2	4	4	517,547	4 (most)

color center is indicative of the size and complexity of the center and hence its sensitivity to high LET (Linear Energy Transfer) radiation. High LET particles, such as protons, alpha particles, etc., deposit more energy per unit pathlength than electrons (low LET radiation) from gamma-ray interactions. This causes greater damage along the particles track and hence the increased sensitivity of the more complex color centers. In the present experiment, neutrons are the only source of high LET particles. The neutron sensitivity of the color centers has been ranked with this in mind. If these assumptions are correct, the absorption peak for R_2 should grow at the expense of M in a neutron field. We shall see that this may be true and that the neutron sensitivity thus could be a determining factor in the use of these dosimetric materials at Climax.

In Figure 1, a drawing made from spectrophotometer traces of some of the calibration dosimeters, the various peaks are evident. The y-axis is in Absorbance Units (A.U.), the negative logarithm to base 10 of the internal transmittance. Significant problems were encountered in use of this standard-type spectrophotometer at very high doses, due to the restricted beam size because of the very small dosimeter. Apertures of 1-mm diameter were used, and special light sources, reference beam attenuators, and alignment procedures were required to produce usable spectra. A simple photometer was eventually adapted for use as a low f-number spectrometer for some of the high dose measurements.

2.1 CALIBRATIONS

The major part of the gamma calibrations was done at the Sandia Gamma Irradiation Facility in Albuquerque through the courtesy of Willis Whitfield. This source is an array of ^{60}Co pins remotely raised into a hot cell. The exposure rates varied from ~1000 to ~85,000 rads-H_2O per minute. All exposures were in air, and all LiF chips were exposed in the stainless steel holders used in the field. Each exposure position was measured with a tissue-equivalent, three-terminal ionization chamber whose calibration is directly traceable to

the NBS. Exposures from 5×10^3 to 5×10^8 rads-H_2O were obtained. Errors are expected to be ±4% or less. For the dosimetry purpose at hand, rads-H_2O and rads-LiF may be treated as interchangeable. (This is clearly not the case for rads-granite as shown in the Appendix. The data presented for USGS-G2 type granite illustrate the importance of the gamma spectral shape when converting the LiF rads to rads-granite. Since neither the elemental makeup of the Climax granite [probably very similar to USGS-G2] nor the gamma spectra were known, the basic data in this report are given in rads-LiF, with the expectation that proper stopping power corrections will be made.)

These exposures resulted in the calibration data plotted in Figure 2. Note that in most regions two or more exposure values can be obtained, since the calibration curves for the various peaks overlap. Some data for the 5-mm path length were also taken and are included for completeness, but they were not used in subsequent analysis.

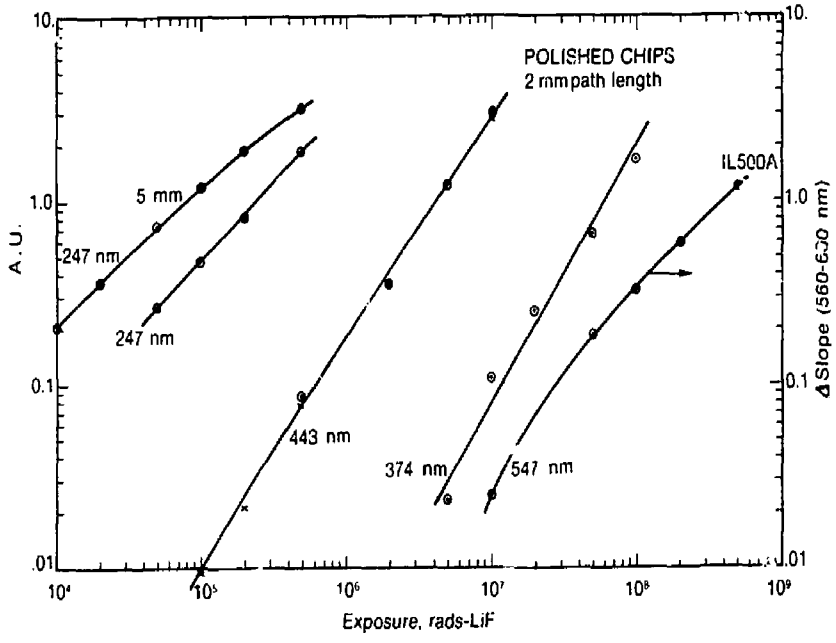

Figure 2. Calibration curves for ^{7}LiF chips, ^{60}Co source

Peaks from these dosimeters as produced on our spectrophotometer were too small to measure accurately below ~0.02 Absorbance Units. Data above 3.0 Absorbance Units were noisy and were used with care when necessary. Note that the various curves are nearly straight lines on the log-log plot similar to previously published data.[3] (The curve marked IL500A will be discussed separately.)

Some data were also taken with unpolished dosimeter chips. These exhibited the same curve shapes and very nearly the identical calibration

values; however, severe problems were encountered at large absorbance values because the additional scattering of light by the rough chip surfaces made measurements unreliable.

The spectrophotometer noise which prevented acquisition of useful data above 3.0 Absorbance Units in turn limited exposures to $\sim 1 \times 10^8$ rads-LiF. Preliminary estimates of gamma rates had shown that exposures greater than 10^8 rads were likely, so some effort was directed toward an improved readout device. A very-close-coupled, manually scanned photometer was available. This, together with a special light source, was converted into a limited-range spectrophotometer suitable for absorbance measurements of the 374 nm peak. The resulting poor resolution, due in part to both the instrument limitations and our efforts to increase photon fluence, prevented use of the 374 nm data as planned. However, it was found that the N_2 band centered at 547 nm was measureable, since the longer wavelength side of the absorbance peak had no noticeable structure, and its slope could be determined accurately. The logarithm of the change in slope with respect to a reference dosimeter behaves similarly to an absorbance value, and is plotted in Figure 2 (marked IL500A) as the other true absorbance data. These Δ slope data are not absolute numbers and are unique to the particular experimental arrangement used.

Because this instrument was modified from its original configuration as a photometer, data were taken to determine its stability versus time. The extensive fade study work (to be described below) allowed many repetitive measurements of the two LiF reference chips over approximately eight months. We found a standard deviation of 2.1% over a total of 32 measurements on both chips. This is adequate for the task at hand.

2.2 FADE STUDIES

Information in the literature[1,2] suggested that this dosimeter system would exhibit very little fade at temperatures up to 50°C over a long-term exposure (several weeks). Some data[2] were available at much higher temperature, 400°C in some cases, but only for a few hours duration. It was necessary therefore to generate long-term fade data at temperatures appropriate to the Climax test environment. For this purpose we prepared pre-irradiated chips, test ovens, and stainless steel holders identical to those used in the field. Two chips each with exposures of 5×10^4, 2×10^6, 5×10^7, and 5×10^8 rads-LiF were baked for 205 days at 50°C, 100°C, and 150°C. An additional group of chips from the calibration work was held at room temperatures over the same time frame. Two unirradiated chips were used as controls. Chips were read out 10 days after start of the test and then approximately monthly thereafter.

In Figure 3, the fade study data, the 25°C room-temperature data have been omitted since no change was observed over the 205 days. The remainder of the Beckman 5270 data show the expected fading with time and temperature. Note that the various exposure levels are represented by data only for the principal absorption peak appropriate for that level. In general, a 100°C environment for 200 days yields fades for 10 to 40%, depending upon the exposure level and hence the peak of interest.

The data from the modified IL500A photometer used to examine the 5×10^7 rad level (same chips as used for the Beckman 5270 data), and an additional set

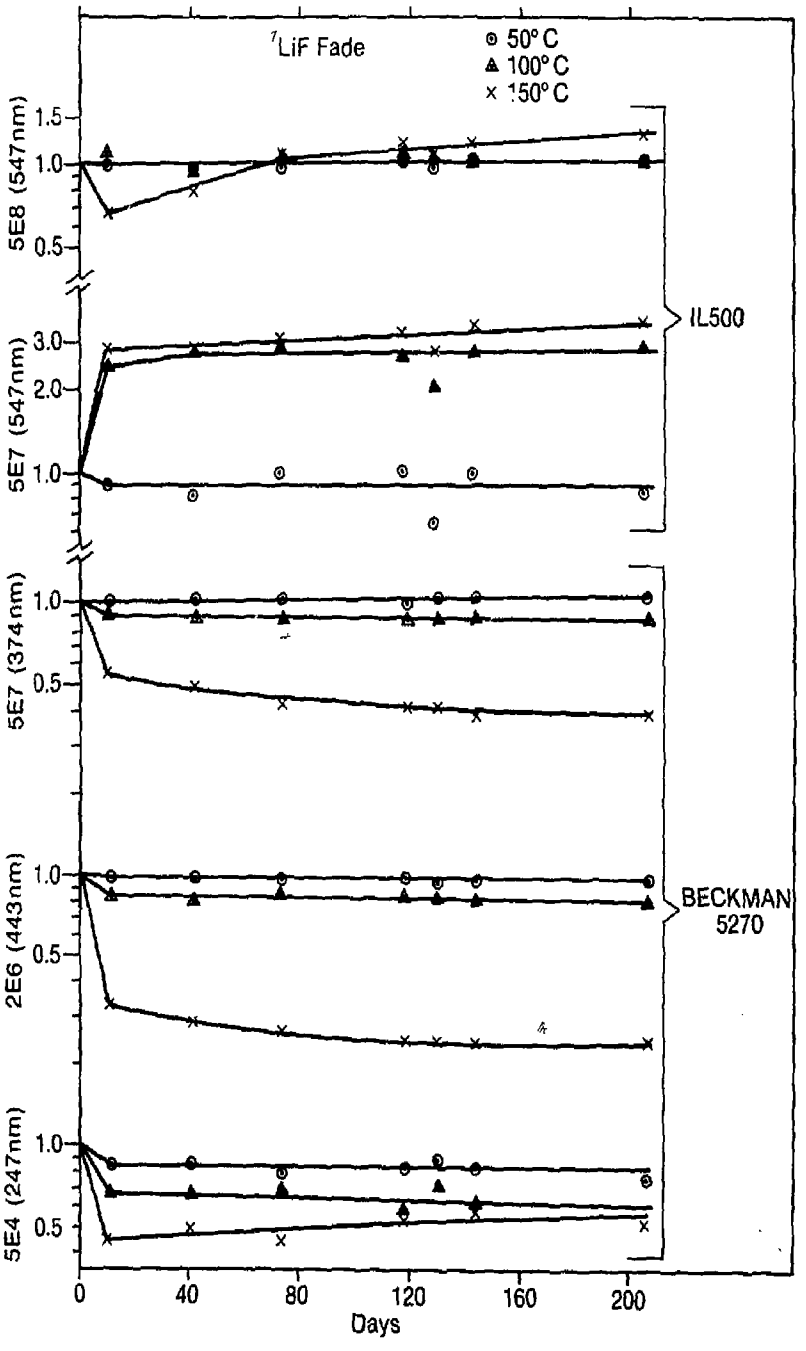

Figure 3. Fade data for ^{7}LiF chips

of chips at the 5×10^8 rad-LiF level, are presented in the upper portion of Figure 3. The 5×10^7 rad level at 50°C seemed to fade similar to the Beckman 5270 data, but higher temperatures of 100° and 150°C produced increased readings. Despite some investigation, these data have not been refuted. It may indicate a transition from the M to the N band, a premise not too well founded though in view of the 5×10^8 rad-LiF data, where only the 150°C data showed a negative fade and then only 20 to 30%. Fortunately, these difficult-to-explain data were not needed for the field experiment.

The relative flatness of the various fade curves after about 40 days elapsed time simplifies the fade corrections considerably. It appears that if one interpolates on temperature using the measured fade data near the end of the test, fade corrections can be calculated with sufficient accuracy. The following equations were obatined by fitting various functional forms to the data (including the 25°C point which showed no fade) for the different peaks. In these equations

Peak, nm	Fade Equation
247	$\text{Fade} = 3.473\ T^{-0.370}$
374	$\text{Fade} = 0.878 + 0.00593T - 0.0000605T^2$
443	$\text{Fade} = 0.892 + 0.00517T - 0.0000632T^2$
IL500A at 5×10^7 rads	$\text{Fade} = 0.152 + 0.0246T - 0.0000109T^2$
IL500A at 5×10^8 rads	$\text{Fade} = 1.12 - 0.00529T + 0.0000428T^2$

a fade value of 1.00 represents no fade, a value of 0.25 represents a decrease in peak height to 0.25 of the original value. The fade-corrected data using temperatures provided by W. Patrick of LLNL[4] are given in Section 4, Field Data.

2.3 NEUTRON SENSITIVITY

At the outset of this experiment a rough calculation from existing data seemed to show that neutrons would not be a significant problem. These data were sketchy however, and ^{7}LiF dosimeters rather than natural lithium were specified to minimize neutron sensitivity. Despite this precaution it appears that some apparent neutron effects have been encountered in the field experiment. This can be seen in Section 4 where the poor agreement between various absorbance peaks is possibly due to greater neutron effects on one peak with respect to another. These effects seem to be related to the size and complexity of the traps responsible for the peak.

Table 1 provided a qualitative picture in that the N_2 color center with a characteristic wavelength of 547 nm is more sensitive to neutrons (actually high LET reaction products) than the 374 nm peak, which in turn is more sensitive than the 443 nm and so on to the 247 nm peak. W.L. McLaughlin[5] of NBS is presently investigating the neutron sensitivity of this dosimetric system, and has provided some preliminary information. These data, shown in Table 2, are subject to change, but they do tend to demonstrate the effects of trap size and complexity on neutron sensitivity. For data presented as n/cm^2 per rad, the smaller the number the fewer neutrons are needed to produce an apparent exposure of one rad, and hence the greater sensitivity to neutrons. Table 2 illustrates the change in neutron

Table 2. n/cm^2 per apparent rad-^{7}LiF

Center	Peak Position (nm)	Neutron Energy Spectrum					
		2 keV	24 keV	144 keV	^{252}Cf	Thermal	Reactor Core
F	247	2.5×10^8	2.3×10^8	2.0×10^8	2.5×10^8	2.0×10^9	--
M	443	--	--	--	2.4×10^8	2.4×10^8	1.4×10^9
N_1	517	--	--	--	--	--	0.3×10^9

sensitivity from $\sim 2 \times 10^8$ n/cm^2 per rad-^{7}LiF for F centers at fission energies to 2×10^9 at thermal energies. This is consistent with a greater effect due to a greater population of high LET particles created in a fast neutron environment. Table 2 also shows that for thermal neutrons the M center is more sensitive than the F center, and for reactor core neutrons the N_1 center is still more sensitive.

A second set of data, also provided by W.L. McLaughlin and given in Table 3, shows a slight trend towards growth of the 443-nm peak (M center) at the expense of the 517-nm peak (N_1 center) in a neutron environment.

Table 3. Absorbance versus neutron exposure for ^{7}LiF (reactor neutrons at 3.1×10^{13} nV)

Time Integrated Fluence	Absorbance		Ratio 443/517
	443 nm	517 nm	
0.4×10^{16}	0.22	0.02	11
1.3×10^{16}	0.72	0.06	12
3.6×10^{16}	1.90	0.18	10.6

It is expected that ^{6}LiF will have a thermal neutron sensitivity at least 900 times greater than that of ^{7}LiF, due mainly to the cross section increase.

As will be seen in Section 4 these neutron sensitivity data are not sufficient to explain the observed effects.

3. NEUTRON DOSIMETRY SYSTEM

3.1 MATERIALS USED

Four principal isotopes were used for neutron fluence measurements: 1) ^{60}Co from the two 0.020-inch-thick cobalt foils and from the 0.216% cobalt in the 303 stainless steel used for the holders, 2) ^{110m}Ag from the two 0.010-inch-thick silver sealing rings, 3) ^{54}Mn from the 71.25% iron in the stainless steel, and 4) ^{58}Co from the 9% nickel in the stainless steel.

The original plan for this experiment included evaluation of some cobalt foils in a token attempt to assess the neutron fluence at various dosimetry locations. During mechanical fabrication of the dosimeter holders, silver was chosen over indium as a soft deformable sealing material, partly because silver's activation product has a long half-life compared to indium. This turned out to be a useful selection. Since the cobalt foils were to be evaluated as a guide to neutron exposure, only a few locations (on the center line) were fitted with foils. In retrospect, it would have been better to have placed these foils at each dosimeter location. However, we were able to use the small percentage of cobalt in the stainless steel to help assign exposures to those locations without the cobalt foils.

The supposedly neutron-caused anomalies in the gamma data prompted a more thorough evaluation of all the parts of each dosimeter holder. Because of the very low activities from many of the isotopes, significant time was spent counting the various items in a low background Ge(Li) detector.[6] Future evaluations will be better prepared for this task.

3.2 ACTIVITY MEASUREMENTS

All parts of each dosimeter holder were counted at least once, most twice, on a low background Ge(Li) detector[6] that is maintained for soil sample analysis. Its calibration is traceable to the NBS via various gamma sources. The resulting data were analyzed with SAMPO,[7] a Gaussian least squares program routinely used for this purpose. The data obtained are presented in Section 4. (The cobalt and silver have been corrected for self-shielding of 0.2 and 0.072, respectively. The dps/nucleus units [see Table 6] are those needed for entry into the spectrum unfold code used for final data analysis.)

3.3 SPECTRAL CALCULATIONS

The saturated activities derived from the Ge(Li) measurements were used as input to CRYSTAL BALL,[8] a spectrum unfold code. In those cases where three or more activation foils were available, spectra were unfolded, differential and integral fluences calculated, and tissue dose calculated. This was done for eight of the 13 locations. Four locations had only two foils with good data. One location, that of the electrical heater, had no detectable activity for any of the foil isotopes.

The unfolded spectral data are very extensive. Each spectrum has 621 energy points and occupies several computer printout pages. Since the detailed neutron data are not of major importance here, they have been summarized in Section 4 as fluence above and below 0.55 eV, the usual cadmium "cut-off" energy. The tissue rad exposures are also given, as well as REM and average neutron energy. Figure 4 is representative of the calculated spectra.

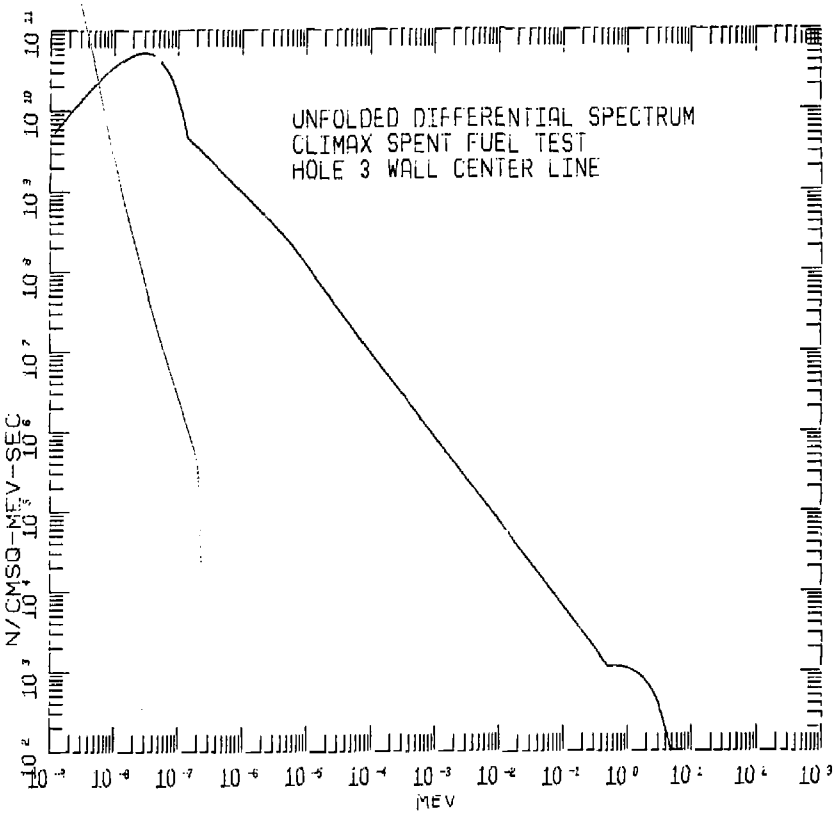

Figure 4. Differential neutron spectrum Hole No. 3, wall, centerline

4. FIELD DATA-CLIMAX TEST

This section presents the gamma and neutron dosimetry data obtained during the ~270-day exposure from April 1980 to January 1981.

4.1 DOSIMETRY LOCATIONS

Dosimeters were installed on the inside wall of five canister emplacement holes, Nos. 1, 3, 4, 7, and 11. Hole No. 3 also had dosimeters placed at radii of 0.51 and 0.66 m from the canister centerline. The locations are listed in Table 4.

Table 4. Dosimeter locations and exposures at Climax Spent Fuel Facility

Hole Number, Dosimeter Location	Vertical Distance From Midplane (m)	^{7}LiF Number	Exposure Time (days)
CEH1 (wall)	+1.22	14	262
	0	15	
	-1.22	16	
CEH3 (wall)	+1.83	7	269
	+1.22	8	
	+0.61	9	
	0	10	
	-0.61	11	
	-1.22	12	
	-1.83	13	
CEH3 (0.51 m)	+1.22	84	269
	0	5	
	-1.22	6	
CEH3 (0.66 m)	+1.22	20	269
	0	21	
	-1.22	22	
CEH4 (heater)	+1.22	1	~242
	0	2	
	-1.22	3	
CEH7 (wall)	+1.22	17	244
	0	18	
	-1.22	19	
CEH11 (wall)	+1.22	23	229
	0	24	
	-1.22	25	

4.2 GAMMA DOSIMETRY DATA

The gamma data derived from the ^{7}LiF chips are given in Table 5. Separate values are tabulated for each readable peak. Based on the quality of the calibration dosimeters one should expect all peaks to yield approximately the same exposure data, which unfortunately is not the case. This is detailed in the Discussion, Section 5.

Table 5. Gamma dosimeter data*

Hole Number, Dosimeter Location	Vertical Distance From Midplane (m)	Exposure, rads-LiF			
		Beckman 5270			IL500A 547 nm
		247 nm	374 nm	445 nm	
CEH1 (wall)	+1.22		3.1×10^{7}	7.3×10^{6}	$2.1 \pm 1.10 \times 10^{7}$
	0		3.6×10^{7}	8.3×10^{6}	$1.9 \pm 1.00 \times 10^{7}$
	-1.22		3.2×10^{7}	6.2×10^{6}	$2.2 \pm 1.10 \times 10^{7}$
CEH3 (wall)	+1.83		1.7×10^{7}	3.8×10^{6}	$9.7 \pm 4.80 \times 10^{6}$
	+1.22		3.4×10^{7}	8.6×10^{6}	$2.4 \pm 1.20 \times 10^{7}$
	+0.61		3.5×10^{7}	9.5×10^{6}	$2.5 \pm 1.20 \times 10^{7}$
	0		3.8×10^{7}	1.0×10^{7}	$2.5 \pm 1.20 \times 10^{7}$
	-0.61		3.8×10^{7}	1.1×10^{7}	$2.6 \pm 1.30 \times 10^{7}$
	-1.22		3.9×10^{7}	>3 A.U.	$3.1 \pm 1.60 \times 10^{7}$
	-1.83		2.0×10^{7}	4.4×10^{6}	$1.3 \pm 0.66 \times 10^{7}$
CEH3 (0.51 m)	+1.22	$5.1 \pm 1.2 \times 10^{5}$		$5.1 \pm 0.2 \times 10^{5}$	
	0	$4.4 \pm 1.1 \times 10^{5}$		$4.5 \pm 0.2 \times 10^{5}$	
	-1.22	$4.3 \pm 1.0 \times 10^{5}$		$4.3 \pm 0.2 \times 10^{5}$	
CEH3 (0.66 m)	+1.22	$9.9 \pm 2.3 \times 10^{4}$		$7.8 \pm 1.0 \times 10^{4}$	
	0	$1.2 \pm 0.3 \times 10^{5}$		$7.7 \pm 0.5 \times 10^{4}$	
	-1.22	$1.3 \pm 0.3 \times 10^{5}$		$8.7 \pm 0.9 \times 10^{4}$	
CEH4 (heater) (wall)	+1.22		8.7×10^{6}	8.0×10^{6}	$8.2 \pm 4.20 \times 10^{6}$
	0		5.2×10^{7}	>3 A.U.	$1.4 \pm 0.15 \times 10^{8}$
	-1.22		>3 A.U.	>3 A.U.	$3.5 \pm 0.38 \times 10^{8}$
CEH7 (wall)	+1.22		3.2×10^{7}	7.9×10^{6}	$2.4 \pm 1.10 \times 10^{7}$
	0		3.3×10^{7}	8.4×10^{6}	$2.2 \pm 1.30 \times 10^{7}$
	-1.22		3.9×10^{7}	1.1×10^{7}	$2.7 \pm 1.10 \times 10^{7}$
CEH11 (wall)	+1.22		3.1×10^{7}	7.4×10^{6}	$2.1 \pm 1.10 \times 10^{7}$
	0		3.3×10^{7}	8.1×10^{6}	$2.0 \pm 1.00 \times 10^{7}$
	-1.22		3.0×10^{7}	7.1×10^{6}	$2.0 \pm 1.00 \times 10^{7}$

*Notes:
1. Data without errors indicated have errors of 3-4% at 2σ. Other indicated errors are at 2σ.
2. Data have been corrected for temperature-induced fade.
3. >3 A.U. means density exceeded measuring range of spectrophotometer.
4. CEH4 had pre-irradiated chips with exposures of 8.5×10^{6}, 5.6×10^{7}, and 2.9×10^{8} given.

The tabulated errors and those in the footnote (Table 5) refer to the precision of the individual determinations. The overall accuracy, traceable to the NBS through our 3-terminal ionization chamber data, is no better than ±4%. Thus the best of the data are ±~6% (exclusive of errors involved in correcting for stopping power between LiF and granite; see the Appendix).

4.3 NEUTRON ACTIVATION FOIL DATA

Table 6 contains the basic activation foil data obtained from the SAMPO fitting code. Corrections have been made for exposure time (lack of saturation), decay to time of counting, and resonance self absorption for the cobalt and silver foils. The large errors seen on many of the foils reflect the low counting rates observed. The Table 6 data were used as input to an iterative unfold code, CRYSTAL BALL, which produces a neutron spectrum that could have caused the set of activities found. The large uncertainties in the input data do not allow a very precise or accurate unfolding, but it has been adequate for similar tasks in the past.

Table 7 presents the results of the spectrum unfolding in those cases where three or more foils were available. A typical spectrum is shown in Figure 4. Much more detail is provided in the basic computer output than is given in this table and is available to the interested reader if needed. (Contact W. Quam, EG&G, Santa Barbara Operations, P.O. Box 98, Goleta, CA 93116.)

Table 6. Activation foil data*

Hole Number, Dosimeter Location	Vertical Distance From Midplane (m)	Saturated dps per Nucleus			
		^{60}Co	^{110m}Ag	^{54}Mn	^{52}Co
CEH1 (wall)	0	1.735 E-19 ±0.0731	8.468 E-20 ±0.1780	1.487 E-22 ±0.1900	1.728 E-22 ±0.1040
CEH3 (wall)	+1.83	1.274 E-19 ±0.4634	5.456 E-20 ±0.0671	--	--
	+1.22	1.733 E-19 ±0.4465	7.490 E-20 ±0.2109	1.527 E-22 ±0.2003	2.356 E-22 ±0.1840
	+0.61	1.878 E-19 ±0.4501	9.446 E-20 ±0.1988	2.109 E-22 ±0.1853	2.700 E-22 ±0.1848
	0	2.002 E-19 ±0.0922	1.015 E-19 ±0.2622	1.677 E-22 ±0.2193	2.495 E-22 ±0.1959
	-0.61	1.935 E-19 ±0.4422	9.028 E-20 ±0.1947	1.880 E-22 ±0.1817	1.953 E-22 ±0.2088
	-1.22	1.987 E-19 ±0.4417	6.151 E-20 ±0.2391	2.404 E-22 ±0.1855	2.058 E-22 ±0.2087
	-1.83	2.330 E-19 ±0.4366	7.624 E-20 ±0.2107	--	--
CEH3 (0.51 m)	0	3.041 E-19 ±0.0734	9.944 E-20 ±0.2436	--	--
CEH3 (0.66 m)	0	1.835 E-19 ±0.0909	5.327 E-20 ±0.3405	--	--
CEH7 (wall)	0	2.962 E-19 ±0.4371	8.738 E-20 ±0.2245	--	2.368 E-22 ±0.2079
CEH11 (wall)	0	1.965 E-19 ±0.4634	1.216 E-19 ±0.2107	--	2.165 E-22 ±0.2367

*Notes: 1. ± figures are fractional errors at 2σ, i.e., 0.0731 is 7.31%. These have been derived from fitting errors and multiple counts.

2. ^{60}Co and ^{110m}Ag have been corrected for self absorption of 0.2 and 0.072 respectively.

3. No activity was detectable for foils at Hole No. CEH4. Lack of other entries in the table means foil activity was too low to be quantifiable.

Table 7. Results of CRYSTAL BALL unfold code*

Hole Number, Dosimeter Location	Vertical Distance From Midplane (m)	Neutron Exposure Rate		E_{AVE} (MeV)	n/cm^2-s	
		rads/s	REM/s		<0.55 eV	<0.55 eV
CEH1 (wall)	0	1.20 E-5	6.70 E-5	0.215	4300	10400
CEH3 (wall)	+1.22	1.62 E-5	1.07 E-4	0.303	4700	11700
	+0.61	1.77 E-5	1.12 E-4	0.292	4900	13700
	0	1.83 E-5	1.17 E-4	0.277	4800	14500
	-0.61	1.35 E-5	7.55 E-5	0.255	5500	11000
	-1.22	1.08 E-5	5.96 E-5	0.271	5000	7280
CEH7** (wall)	0	1.76 E-5	1.06 E-4	0.242	8200	11800
CEH11** (wall)	0	1.78 E-5	1.06 E-4	0.223	5800	15000

*Errors on unfolded data are probably no better than ±30%.
**Three foils only.

5. DISCUSSION

This work was undertaken to verify the gamma exposure values in the Climax Spent Fuel Test environment. Table 5 in the report provides the best estimates of these exposure values. If we disregard the 547-nm data for the moment the remaining data are internally inconsistent except for the six dosimeters at the lowest exposures, at 0.51 m and 0.66 m from the fuel element in CEH3, which show reasonable agreement (at 2σ). The remaining dosimeters, all at higher exposures, consistently show the 374-nm data to be significantly higher than the 443-nm data. These facts seem to be consistent with a neutron-caused effect, since the 374-nm peak should be much more sensitive than the other two.

The known neutron sensitivities (Tables 2 and 3) for ^{7}LiF are not large enough to cause the observed differences. It may be possible that ^{6}LiF would have a large enough neutron sensitivity to be significant here, but if one plots the "excess" exposure observed at 374 nm over that at 443 nm there is no trend with either thermal, fast, or total neutron population. It appears that something other than neutrons alone is the cause of the differences observed. Extensive re-measurement of the chips has not shown any anomolies. The temperature-induced fade corrections are significant but are not large enough in absolute value to be the cause if they are in error. Perhaps there is a synergistic effect between temperature and neutron fluence.

The CEH3 locations at 0.51 and 0.66 m from the canister centerline have approximately the same neutron fluence as the other sites, but they are slightly lower in temperature than most. There is no obvious trend among the six sets of data that can be traced to neutron fluence levels or temperature. Therefore, it is reasonable to expect the remaining 443-nm data to be unaffected (to the same degree) by the neutron fluences encountered at the other measurement sites. The remaining question is: What is the effect of a higher temperature on the 443-nm data in the presence of a neutron fluence? No data are available to evaluate this (supposed) effect. It is recommended that the 247- and 443-nm data be used for dosimetry purposes. Given the apparent increases of the 374-nm peaks caused by the environment at Climax, it seems reasonable to assume that the 443-nm data are an upper limit to that actually encountered.

The 547-nm data, obtained with a different readout technique, show unexpected changes in fading with temperature, particularly in the ranges where most of the data occur. A more extensive fading study may resolve these uncertainties, but for now it seems best to eliminate these data from consideration. This peak also should show the most effects from neutron interactions and thus would suffer from that additional interpretive difficulty.

The chips exposed in the heater hole, CEH4, were given exposures before placement in the field. The Table 5 data show there is reasonable agreement between all three peaks for the one chip where all peaks were readable. The 374-nm data are also in good agreement with the measured pre-placement values (Note 4, Table 5) for exposures $<10^{8}$ rads-LiF. The 443-nm point also shows reasonable agreement with the pre-placement data. No neutrons were detected

by the dosimetry in hole CEH4. Thus the agreement between the various peaks in this case may support the contention that neutrons have contributed to the disagreement discovered in the other sets of data.

In conclusion, the 247-, 374-, and 443-nm peaks are expected to provide the best data. The disagreement between the 374- and 443-nm data (a factor of 4) at those locations near fuel elements is unexplained. It may be due to neutron plus heat synergistic effects, or perhaps to the varying color sensitivity during irradiation at elevated temperature. The resolution of this disagreement is under study.

REFERENCES

1. McLaughlin, W.L., et al, "Electron and Gamma-Ray Dosimetry Using Radiation-Induced Color Centers in LiF," paper given at the Second International Meeting on Radiation Processing, Miami, Florida (October 1978).

2. Lucas, A.C. and B.M. Kapsar, "Fading of M, R, and N Centers in Pure LiF Megarad Dosimeters," unpublished paper, Harsaw Chemical Company (1980).

3. Vaughan, W.J. and L.O. Miller, "Dosimetry Using Optical Density Changes in LiF," *Health Physics, 18*, 578 (1970).

4. Patrick, W.C., letter dated 20 March 1981 providing thermal histories of dosimeter locations.

5. McLaughlin, W.L., private communication, 11 June 1981.

6. Quam, W. and K. Engberg, "Low Background Ge(Li) Detector with Anticoincidence NaI Annulus (2nd Revision)," EGG 1183-2326 (Rev.) (February 1976).

7. Routti, J. and S.G. Prussin, "Photopeak Method for the Computer Analysis of Gamma-Ray Spectra from Semiconductor Detectors," *NIM, 72*, 125-142 (1969).

8. Kam, F.B.K., and F.W. Stallman, "Crystal Ball — A Computer Program for Determining Neutron Spectra from Activation Measurements," ORNL-TM-4601 (1974).

APPENDIX: STOPPING POWER OF GRANITE

Energy deposition in a material is dependent upon its elemental composition and the incident gamma-ray energy. At any one energy the following equation applies:

$$\text{rads}_{\text{granite}} = \frac{\left(\mu_{en}/\rho\right)\ \text{granite}}{\left(\mu_{en}/\rho\right)\ \text{LiF}} \times \text{rads}_{\text{LiF}}$$

The following table presents values of μ_{en}/ρ* calculated for USGS-G2 granite composition and for LiF at three different energies. The values of μ_{en}/ρ were taken from Storm and Israel, LA-3753. Proper application of data of this type must take into account the gamma energy spectrum at the point under consideration. Significant attenuation effects are to be expected in the stainless steel around the fuel and in the granite itself. This may be particularly important at the emplacement hole wall.

*The "mass energy-absorption coefficient," μ_{en}/ρ, is a weighted sum of the probability per unit path length for photoelectric absorption, Compton collision, and pair production. The weights account for the escape of photons from Compton-scattering, fluorescence, annihilation, and bremsstrahlung interactions. Additional comments on μ_{en}/ρ can be found in paragraph 17 of Appendix 1 of NBS Handbook 85, and in Section 1.5 of NSRDS-NBS 29 "Photon Cross Sections, Attenuation Coefficients, and Energy Absorption Coefficients from 10 keV to 100 GeV."

Granite USGS-G2

Element	Composition	μ_{en}/ρ, cm^2/g		
		10 keV	100 keV	1 MeV
H	0.000733	0.0129	0.0406	0.0554
C	0.000218	1.91	0.0211	0.0279
O	0.4891	5.31	0.0228	0.0279
F	0.001290	7.54	0.0231	0.0263
Na	0.0302	14.9	0.0280	0.0265
Mg	0.00458	20.3	0.0324	0.0275
Aℓ	0.0817	25.7	0.0362	0.0268
P	0.000611	39.7	0.0482	0.0268
K	0.0374	77.0	0.0895	0.0271
Ca	0.0139	89.1	0.107	0.0278
Ti	0.00300	101.0	0.129	0.0255
Mn	0.000263	127.0	0.190	0.0254
Fe	0.01885	139.0	0.219	0.0260
Rb	0.000168	53.9	0.586	0.0249
Sr	0.000479	59.1	0.634	0.0250
Fr	0.000300	70.0	0.726	0.0255
Be	0.00187	173.0	1.50	0.0268
Ce	0.000150	193.0	1.62	0.0279
Th	0.000024	168.0	1.38	0.0428
U	0.000002	180.0	1.49	0.0440
Σ	1.00	23.423	0.04222	0.02786
LiF				
Li	0.2664	0.141	0.0176	0.0240
F	0.7336	7.54	0.0231	0.0263
Σ	1.00	5.569	0.02163	0.02569
$\frac{rads_{granite}}{rads_{LiF}}$		4.206	1.952	1.084

DISTRIBUTION

USDOE, NVO

J.A. Koch
R.R. Loux
J. Newlin

USDOE, TIC, Oak Ridge

T.B. Abernathy (2)

LLNL

Distribution per
attached list

EG&G, LVO

T.O. Edwards
Library

EG&G, SBO

T. DeVore
W. Quam (10)
Library
Publications (2)

Distribution List for "Climax Spent Fuel Dosimetry -- Progress Report" by W. Quam and T. Devore

Headquarters

C. R. Cooley
Office of Waste Isolation
U.S. Department of Energy
Washington, DC 20545

C. A. Heath
Office of Waste Isolation
U.S. Department of Energy
Germantown, MD 20767

R. Stein
Office of Waste Isolation
U.S. Department of Energy
Washington, DC 20545

Columbus

S. J. Basham
Engineering Development
Office of Nuclear Waste Isolation
Battelle Memorial Institute
505 King Avenue
Columbus, NV 43201

W. Carbiener
Technology Development Department
Office of Nuclear Waste Isolation
Battelle Memorial Institute
505 King Avenue
Columbus, OH 43201

J. A. Carr
Engineering Development
Office of Nuclear Waste Isolation
Battelle Memorial Institute

S. Goldsmith
Office of Nuclear Waste Isolation
Battelle Memorial Institute
505 King Avenue
Columbus, OH 43201

J. F. Kircher
Office of Nuclear Waste Isolation
Battelle Memorial Institute
505 King Avenue
Columbus, OH 43201

S. C. Matthews
Office of Nuclear Waste Isolation
Battelle Memorial Institute
505 King Avenue
Columbus, OH 43201

J. O. Neff
Office of Waste Isolation
Columbus Program Office
U.S. Department of Energy
Columbus, OH 43201

Las Vegas

M. P. Kunich
Waste Isolation Branch
Engineering & Energy Applications Division
Nevada Operations Office
Department of Energy
P.O. Box 14100
Las Vegas, NV 89114

R. M. Nelson
Nevada Nuclear Waste Storage Investigation
Nevada Operations Office
P.O. Box 14100
Las Vegas, NV 89114

Mercury

A. R. Hakl
Westinghouse Electric Corp/AESD
NTS, Area 25, M/S 703
P.O. Box 708
Mercury, NV 89023

Aiken

A. Thomas
Interim Spent Fuel Management Group
E. I. Du Pont
Savannah River Plant
Aiken, S.C. 29808

Upton

P. W. Levy
Brookhaven National Laboratory
Upton, New York 11973

Denver

G. L. Dixon
U. S. Geological Survey
Box 25046
Denver Federal Center
Denver, CO 80225

Los Alamos

B. R. Erdal, M/S 514
Los Alamos National Laboratory
P.O. Box 1663
Los Alamos, NM 87545

D. C. Nelson, M/S 985
Los Alamos National Laboratory
Los Alamos, NM 87545

Albuquerque

J. K. Johnstone
Org. 4537
Sandia National Laboratory
Albuquerque, NM 87185

R. W. Lynch
Sandia National Laboratory
Org. 4530
Sandia National Laboratory
Albuquerque, NM 87185

L. W. Scully
Org. 4531
Sandia National Laboratory
Albuquerque, NM 87185

L. D. Tyler
Org. 4538
Sandia National Laboratory
P.O. Box 5800
Albuquerque, NM 87185

Pittsburgh

J. B. Wright
Westinghouse Electric Corporation
Advanced Energy Systems Division
P.O. Box 10864
Pittsburgh, PA 15236

Richland

D. J. Bradley
Battelle Pacific Northwest Laboratory
P.O. Box 999
Richland, WA 99352

R. E. Einziger, H-A6
Bldg. 323/Trailer 1
Hanford Engineering Development
P.O. Box 1970
Richland, WA 99352

Kunsoo Kim
Basalt Waste Isolation Project
Rockwell Hanford Operations
P.O. Box 800
Richland, WA 99352

LLNL

L. Ballou, L-204
R. Carlson, L-222
W. Durham, L-201
D. Montan, L-200
W. Patrick, L-204
A. Rothman, L-204
R. Van Konynenburg, L-396
T. Wilcox, L-45